Wear and stability analysis of the train-curve rail system with an elastic anti-friction guard rail

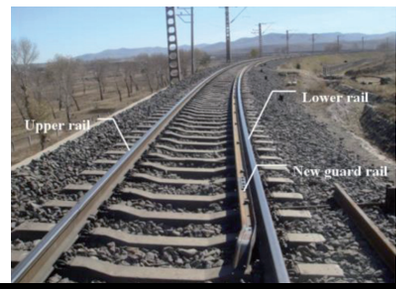

ANÁLISIS DE DESGASTE Y ESTABILIDAD DEL SISTEMA EN LA CURVA FERROVIARIA INCORPORANDO UN GUARDA RAÍL ANTIFRICCIÓN ELÁSTICO

DOI: http://dx.doi.org/10.6036/7630 | Recibido: 20/apr/2015 • Aceptado: 10/jun/2015

Jianhong Mao[1,2], Jun Xiang[1,*], Cuiying Yu[1], Xiangming Liu[3] and Kai Gong[1]

[1] School of Civil Engineering, Central South University, Shaoshan South Road 22#, Changsha, 410075, Hunan, China, jxiang@mail.csu.edu.cn

[2] School of Civil and Architectural Engineering, East China Jiaotong University, East Shuanggang Street 808#, Nanchang , 330009, Jiangxi, China

[3] Section of Railway Engineering, Civil Engineering and Geosciences, Delft University of Technology, Stevinweg 1, 2628CN, Delft, the Netherlands

RESUMEN

- Se ha establecido un nuevo modelo para analizar la vibración espacial de un sistema tren – rail en curva con nuevo guardarraíl, basado en el modelo de análisis de vibraciones espaciales del sistema tren-vía, y conforme a las características estructurales del nuevo guardarraíl. La ecuación matricial del sistema dinámico de acoplamiento tren–rail en curva con el nuevo guardarraíl se establece de acuerdo con la dinámica de energía potencial total constante de un sistema elástico y a la existencia del principio de "colocación en posición correcta" del conjunto del sistema. El correspondiente programa de cálculo fue compilado con el lenguaje FORTRAN. Las respuestas de las vibraciones espaciales del sistema tren-rail con guardarrail se han calculado en tres condiciones, concretamente con espaciado de 65, 70 y 75 mm entre la nueva guía de protección y el raíl interno. La exactitud del modelo ha sido verificada a través de una prueba de campo. Los resultados del cálculo demuestran que la diferencia de resultados entre la fuerza horizontal máxima calculada en el guardarraíl y el valor medido alcanzaba el 99,55%, 99,60% y 98,82%, respectivamente, en las tres condiciones. Mientras tanto, otros resultados, como el desplazamiento lateral del guardarraíl y el raíl exterior, están cerca de los resultados medidos. El gran efecto del guardarraíl se observó también en la condición de espaciado de 65 mm. En este caso, el nuevo guardarraíl puede reducir el 14,64% del desplazamiento lateral respecto al raíl exterior y mejorar la estabilidad en la marcha del convoy. Cuando los radios de curvatura son de 250, 300, 350, 400, 450, 500 y 600 m, el nuevo guardarraíl soporta el 39,94%, 38,81%, 36,71%, 35,88%, 34,87%, 33,58% y 33,10%, respectivamente, de la fuerza horizontal del raíl exterior. Esto es acorde con los resultados de los ensayos de que el nuevo guarda raíl puede compartir entre 33,3% - 40% de la fuerza lateral del raíl exterior de la curva.
- **Palabras clave:** nuevo guardarraíl, raíl en curva, convoy ferroviario, análisis de vibraciones, ingeniería ferroviaria.

ABSTRACT

A new model to analyze the spatial vibration of a train-curve rail system with a new guard rail was established based on the spatial vibration analysis model of a train-track system, and in accordance with the structure characteristics of the new guard rail. The matrix equation of the train-curve rail dynamic coupling system with a new guard rail was set up in accordance with the constant total potential energy of elastic system dynamics and the "sit-in-right-position" principle of system matrix formation. The corresponding calculation program was compiled with FORTRAN language. The space vibration responses of the train-rail with a guard rail system were calculated under three conditions, namely, flange way widths of 65, 70, and 75 mm between the new guard rail and the inner rail. The model accuracy was verified through a field test. Calculation results demonstrated that data matching between the calculated maximum horizontal force of the guard rail and the measured value reached as high as 99.55%, 99.60% and 98.82% under the three conditions, respectively. Meanwhile, other calculation results, such as the lateral displacements of the guard rail and the outer rail, are close to the measured results. The great effect of the guard rail under the condition of flangeway width with 65 mm is also observed. In this case, the new guard rail can reduce 14.64% of the lateral displacement of the outer rail and improve the riding stability of the freight train. When the radius of the changing curve are 250, 300, 350 , 400, 450, 500 and 600 m, the new guard rail undertakes 39.94%, 38.81%, 36.71% , 35.88%, 34.87%, 33.58% and 33.10% ,respectively, of the horizontal force of the outer rail. This agrees with the test result that the new guard rail could share 33.3%–40% flange force of the outer rail of the curve.

Keywords: new guard rail, curve rail, freight train, vibration analysis, railway engineering.

1. INTRODUCTION

Derail causes damage to the track structure, traffic suspension, or even a car crash. Derail accident happens occasionally at a small-radius curve track, resulting in serious abrasion and failure, poor lateral stability, heavy maintenance load, and high operating cost. To address these problems, the China Academy of Railway Sciences and associated railway administrations developed a new guard rail device against derail at small-radius curve rail. This guard rail device is generally installed at the inner side of the lower rail (Fig.1). According to years of engineering practice, this new guard rail device has good derailment prevention, wear reduction performance, and stability augmentation.

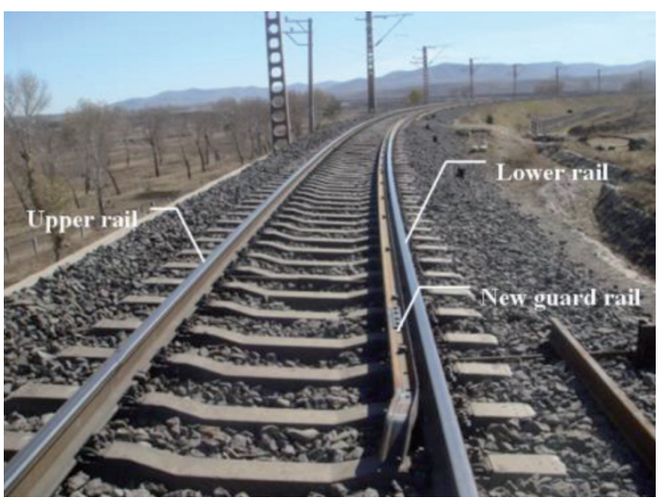

Fig. 1: Site photos of the new guard rail

However, the performance of this new guard rail was mainly analyzed through experiments, field observation, and statics method. For example, Li Zhongcai et al.[1] studied the performance of the new guard rail through field test and obtained valuable conclusions on the flangeway width of the guard rail, guard rail force, and guard rail pavement scope. Through an experimental study, Ran Lei et al.[2] pointed out the bearable lateral deformation and horizontal force of the guard rail on an urban viaduct. Chen Xishun[3] calculated the static flangeway width of a guard rail based on the contact status between the wheel track. Wu Fenglin et al.[4] established the three-dimensional finite element model of the new guard rail using SPA91 static and dynamic structural analysis software. They analyzed stresses on the special support system and improved weak parts. However, no research has yet to report on the space vibration model of the train-curve rail system with a new guard rail and its dynamic simulation. Scholars in the area of vehicle-track coupling dynamics conducted extensive research, and a lot of good research results have been obtained [5-10], however, does not consider the role of new guard rail. Hence, there is no theoretical guidance and corresponding standard for the new guard rail although it has been used for many years. As a result, this paper conducted a dynamic simulation analysis on the train-curve rail system with the new guard rail, with the aims of disclosing its derail prevention and antifriction mechanisms, exploring its key parameters, and formulating some standards. Research results are of important theoretical and practical significance.

In this paper, a dynamic simulation and calculation model of the train-rail system with a new guard rail was established by adding the new guard rail into the rail model in accordance with the analysis methods of the spatial vibration of the train-track system[11-12]. Influence law of the new guard rail on the spatial vibration response of the train-track system was discussed. The results help lay a solid theoretical foundation for further understanding the derail prevention, antifriction, and stability augmentation mechanisms of the new guard rail.

2. TRAIN-CURVE RAIL SYSTEM MODEL WITH NEW GUARD RAIL

2.1. SPATIAL VIBRATION ANALYSIS MODEL OF THE TRAIN

The new guard rail device is installed in the curve rail structure and will not influence the vehicle model. The vehicle model is established according to previously reported methods [11–12]. Haulage motor, loaded car and empty car are all discretized into multi-rigid-body system with secondary suspension. Both car body and bogie take six degrees of freedom (DOFs) into account, including flexibility, yaw, drifting, side rolling, nodding, and shaking. Each wheel only considers two DOFs: yaw and drifting. This way, each vehicle has 26 DOFs. The total potential energy (Π_{vi})of the space vibration of each vehicle can be deduced.

2.2. ANALYSIS MODEL OF THE SPATIAL VIBRATION OF THE RAIL-NEW GUARD RAIL

2.2.1. Unit model of the spatial vibration section of the rail- new guard rail

The new guard rail is mainly composed of guard rail, special guard rail support, connectors, and fastening parts (Fig.2). The guard rail is fixed tightly on the special guard rail support by bolts. The support is fastened on the inner rail flange between two ties (or back-up blocks) by buckle plates and bolts. The new guard rail is not connected directly with the sub-rail track bed (tie)[13].

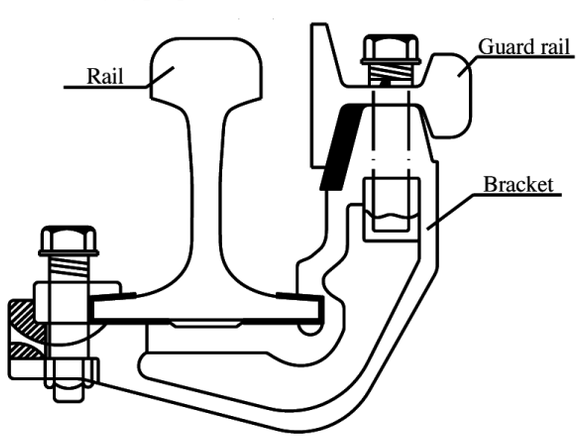

Fig. 2: Structural map of the new guard rail

Based on the structural characteristics of the new guard rail device, the unit model of rail-new guard rail spatial vibra-

tion section with 42 DOFs was built by adding the new guard rail device into the curve rail model (Fig.3). In this model, rails (R_l, R_p) and guard rail (G) are simulated as continual elastic supporting the Euler beam; sleepers (S) are regarded as a short elastic foundation beam; rail fasteners are considered linear springs and dampers; and guard rail bracket is simulated as linear springs and dampers set in every two sleepers.

This unit model is based on several basic assumptions listed below.

(1) The rail is divided into two layers and the vibration of the track bed is neglected.
(2) The tie is directly placed on the elastic track bed. Here, the vertical spring coefficients of the track bed are K_0 and K_1, and the damping coefficients are C_0 and C_1. The transverse elasticity and damping coefficients are K_2 and C_2, respectively, while the vertical spring and damping coefficients are K_3 and C_3, respectively.
(3) Both stock rail and guard rail are simulated as elastic bearing Euler beams. The stock rail is connected to the tie by fasteners. Fasteners are simulated as linear spring and viscous damper. Their vertical elasticity and damping coefficients are K_4 and C_4, respectively, while their transverse elasticity and damping coefficients are K_5 and C_5, respectively. The parameter values are indicated in References [11, 12].
(4) The guard rail is directly connected with the stock rail using a special support. The special support is simulated as linear spring and viscous damper. Its vertical elastic and damping coefficients are K_6 and C_6, respectively, and its transverse elastic and damping coefficients are K_7 and C_7, respectively. The parameter values are presented in Reference [4].
(5) The tie is viewed as an elastic deformation body, but its axial deformation and torsional deformation are neglected.
(6) The unit coordinates are within the rail plane. The X-axis is the curvilinear coordinate of the rail center line, the Y-axis is the radial coordinate, and the Z-axis is the vertical coordinate. The radius of curvature of the X-axis is R and the elevation of the outer rail is Δh.

Displacement simulation at unit node on the associated rail section is described by the parameters given by:

$$\{\delta\}_e = \begin{Bmatrix} \{\delta_1\} \\ \{\delta_2\} \end{Bmatrix}_{42\times1} \tag{1}$$

Where 1 and 2 represent unit left and right node, respectively. In the equations below:

$$\{\delta_1\} = \left[U^T_{1R}, V^T_{1R}, W^T_{1R}, \theta^T_{X1R}, \theta^T_{Y1R}, \theta^T_{Z1R}, \varphi^T_{1R}, U^T_{1L}, V^T_{1L}, W^T_{1L}, \theta^T_{X1L}, \theta^T_{Y1L}, \theta^T_{Z1L}, \varphi^T_{1L}, V^S_1, W^S_{1R}, W^S_{1L}, V^H_1, W^H_1, \theta^H_{Y1}, \theta^H_{Z1}\right] \tag{2}$$

$$\{\delta_2\} = \left[U^T_{2R}, V^T_{2R}, W^T_{2R}, \theta^T_{X2R}, \theta^T_{Y2R}, \theta^T_{Z2R}, \varphi^T_{2R}, U^T_{2L}, V^T_{2L}, W^T_{2L}, \theta^T_{X2L}, \theta^T_{Y2L}, \theta^T_{Z2L}, \varphi^T_{2L}, V^S_2, W^S_{2R}, W^S_{2L}, V^H_2, W^H_2, \theta^H_{Y2}, \theta^H_{Z2}\right] \tag{3}$$

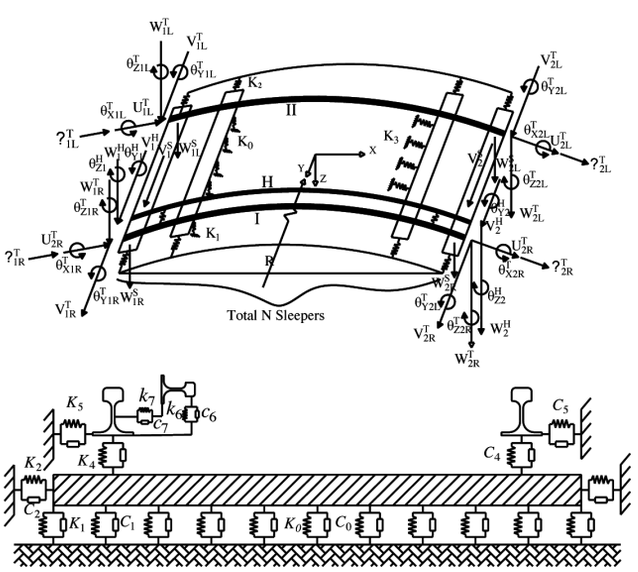

Fig. 3: Aerial and profile views of the spatial vibration model of the curve track with the new guard rail

T represents rail displacement; S is tie displacement; H is guard rail displacement; R is right; L is left; U, V, W, and θ are the linear displacement and angle displacements along the X, Y and Z directions, respectively; V^s_1, W^s_{1R}, W^s_{1L} are the displacements of the first tie at the Y direction as well as its displacement at the right and left connection points with the rail on the Z direction, respectively; and V^s_2, W^s_{2R}, W^s_{2L} are the displacement of the Nth tie at the Y direction as well as its displacement at the right and left connection points with the rail on the Z direction, respectively. The change rate parameters of torsion angle along the X direction φ^T_{1R}, φ^T_{2R}, φ^T_{1L}, φ^T_{2L} are added in the rail node displacement to express the constraint torsion (buckling deformation) of the rail.

2.2.2. Total potential energy of rail–new guard rail space vibration (Π_{TH})

Elastic deformation energies and inertia potential energy of the rail and tie as well as the elastic deformation energy and damping potential energy of rail fasteners are derived from the rail displacement mode. By adding them, the total potential energy of space vibration of the i^{th} rail unit (Π_{Ti})can be obtained. The elastic deformation energy and inertia potential energy of the guard rail, as well as the elastic deformation energy and damping potential energy of the guard rail support are derived from the displacement mode of the guard rail. By adding them, the total potential energy of space vibration of the i^{th} guard rail unit (Π_{Hi})can be obtained. Meanwhile, if we add Π_{Ti} and Π_{Hi}, the total potential energy of space vibration of the i^{th} rail-new guard rail unit (Π_{TH}) can be obtained. Suppose there are N rail units in the calculation range. Then, the total potential energy of space vibration of the whole rail-new guard rail structure (Π_{TH}) is given by:

$$\Pi_{TH} = \sum_i^N \left(\Pi_{Ti} + \Pi_{Hi}\right) \tag{4}$$

2.3. THE TRANSVERSE IMPACT POTENTIAL ENERGY OF THE GUARD RAIL AND THE TRANSVERSE FLANGE FORCE POTENTIAL ENERGY OF OUTER RAIL

When train passes through the curve rail with the new guard rail, the interaction force between the inner wheel back and the guard rail can be simulated into a spring force, which is called the guard rail force (F_g).The interaction force between the outer wheel flange and the outer rail can also be simulated into a spring force, which is called the flange force (F_f). Reference [11] has made similar simulations. The contact spring stiffness between the inner wheel back and the guard rail is k_g ,and that between the outer wheel flange and the outer rail is k_f (Fig.4). Now, the potential energies of F_g and F_f can be calculated.

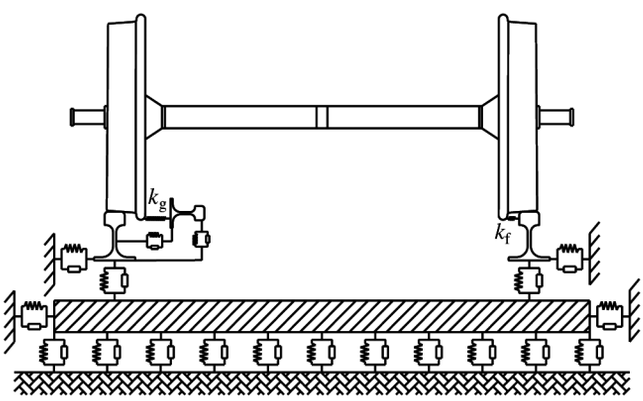

Fig. 4: Profile view of the spatial vibration model of the curve track with the new guard rail

(1) Potential energy of the transverse impact of the guard rail (Π_{Fg})

The calculation of F_g and F_f is mainly based on that presented in previous works [14–15]. The computation process is expressed as:

$$F_g = \begin{cases} k_g \cdot \Delta_g, & \Delta_f \geq 0 \\ 0 & \Delta_f < 0 \end{cases} \tag{5}$$

where $\Delta_g = y_w + \delta/2 + d - (y_g + \Delta)$, y_w is the lateral displacement of wheel set, δ is wheel-rail slack, d is the thickness of flange, y_g is the lateral displacement of guard rail, and Δ is the flangeway width of guard rail. Then, Π_{Fg} is expressed as:

$$\Pi_{Fg} = \frac{1}{2} \times F_g \times \Delta_g \tag{6}$$

(2) Potential energy of the lateral flange force of the outer rail (Π_{Ff})

After the inner wheel back interacts with the guard rail and the guard rail produces small deformation, the outer wheel flange also comes into contact with the outer track rail head of the curve, thus generating the lateral flange force of the outer rail. Its calculation formula is given by:

$$F_f = \begin{cases} k_f \cdot \Delta_f, & \Delta_f \geq 0 \\ 0 & \Delta_f < 0 \end{cases} \tag{7}$$

Where $\Delta_f = y_w - (y_{or} + \eta_{or} + \delta/2)$, in which y_{or} is the lateral displacement of the outer rail, and η_{or} is the lateral irregularity of the outer rail. Then, the potential energy of flange force of the outer rail can be computed using:

$$\Pi_{Ff} = \frac{1}{2} \times F_f \times \Delta_f \tag{8}$$

2.4 ESTABLISHING AND SOLVING SYSTEM SPACE VIBRATION EQUATION

Suppose there are M trains within the calculation range at t, and the total potential energy of train vibration is given by:

$$\Pi_V = \sum_{I}^{M} \Pi_{Vi} \tag{9}$$

Then, the total potential energy of the space vibration of the train-curve rail system with new guard rail at t is expressed as:

$$\Pi_d = \Pi_V + \Pi_{TH} + \Pi_{Fg} + \Pi_{Ff} \tag{10}$$

The matrix equation of the system space vibration at t can be obtained according to the constant total potential energy of elastic system dynamics and the "sit-in-right-position" principle of the system matrix forming [16].

$$[M]\{\ddot{\delta}\} + [C]\{\dot{\delta}\} + [K]\{\delta\} = \{P\} \tag{11}$$

Where $[M]$, $[C]$, and $[K]$ are the mass, damping and stiffness matrices of system space vibration, respectively, and $[\ddot{\delta}]$, $[\dot{\delta}]$, $[\delta]$, and $[P]$ are the acceleration, speed, displacement and load arrays of the system, respectively. The vertical irregularity of the rail is taken as the excitation source for the stochastic analysis of the vertical system vibration, while the artificial s-shaped wave of train framework is used as the excitation source for stochastic analysis of horizontal system vibration. FORTRAN language was also used to compile corresponding calculation program. *wilson - θ* is used to solve this equation.

3. VERIFICATION

The China Academy of Railway Sciences and the Beijing Railway Bureau cooperated to install the new guard rails at the curve rails Beijing-Baotou uplink K242+322~K242+842. The dynamics of the new guard rail was tested based on travelling freight trains [17]. The range of flangeway width affecting the new guard rail was analyzed by setting three distances (flangeway widths of 65, 70 and 75 mm, respectively) between the new guard rail track and the inner curve. In order to validate the proposed model, the space vibration response of the freight train-curve rail system with the new guard rail device was calculated on the basis of the aforementioned three flangeway widths (65, 70, and 75 mm) and on experimental parameters. The calculated results were compared with the test results. The calculation conditions and parameters are as follows: (1) all freight trains are composed of both empty and loaded cars. In other words, one engine drives three loaded cars and two empty cars. They are all C62 open cars. (2) The

calculated line length is 500 m, including a 40 m straight line, a 60 m curve line, a 300 m circular curve line, a 60 m easement curve line, and a 40 m straight line. Values of the guard rail stiffness (k_h)were determined according to test results shown in a previous study [4]. The values of k_g and k_f were determined according to the reference test reports [17]. Other parameters are listed in Table 1.

Parameter		Parameter	
Curve radius /m	297	Vehicle speed /km/h	68
Elevation of curve /m	0.125	Clacking of curve gauge /mm	10
wheel-rail slack/mm	18		

Table 1 Calculation parameters

The theoretical maximum values of the following indexes can be calculated under three conditions. The comparison of their measured values is shown in Table 2.

As shown in Table 2, the calculation results of all indexes highly conform to the measured results. The transverse impact of the guard rail shows the highest matching degree between the calculated maximum and the measured maximum, reaching as high as 99.55%, 99.60% and 98.82% in the three cases, respectively. The matching degrees of the flange force are 91.26%, 97.03% and 99.03%, respectively. Meanwhile, other calculation results, such as the lateral displacements of the guard rail and the outer rail, are close to the measured results. Therefore, the accuracy and feasibility of the established calculation model are confirmed by comparing the calculation results of the three conditions with the experimental results. The test and calculation results also indicate that the lateral force of the guard rail is reduced as flangeway width increases, whereas that of the outer rail increases. When the flangeway width is 75 mm, the measured guard rail shares only 9.33% of the flange force, Meanwhile, when the flangeway width is 65 mm, the measured guard rail shares 36.60% of the flange force. Therefore, in the three groups of test results, the performance of guard rail can be better developed when the flangeway width is 65 mm. Hence, the flangeway width with 65 mm was selected for the subsequent section spatial vibration analysis of the system.

4. CALCULATION RESULTS AND PARAMETER ANALYSIS

To explore the effects of the new guard rail device on some response indexes in the train-rail space system, train-rail system space vibration responses with and without guard rail were calculated under the test conditions and using calculation parameters the flangeway width was set to 65 mm. Limited by the article length, calculation results of only the 4th car were involved and system vibration response indexes mainly included F_g, F_f, y_g, y_{or}, and y_c and lateral Sperling stability. On this basis, variation laws of guard rail force and flange force of the outer rail against the curve radius were analyzed.

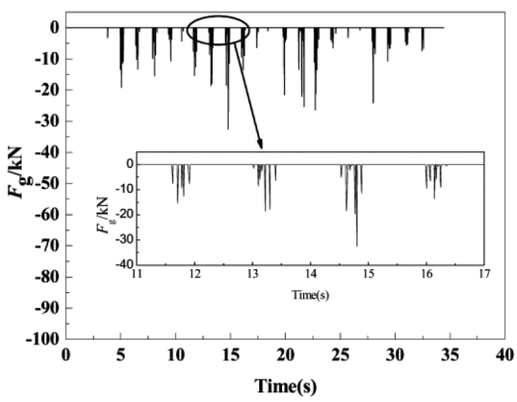

Fig. 5: Transverse force waveforms of the 1st-axis inner wheels of the 4th car on the guard rail

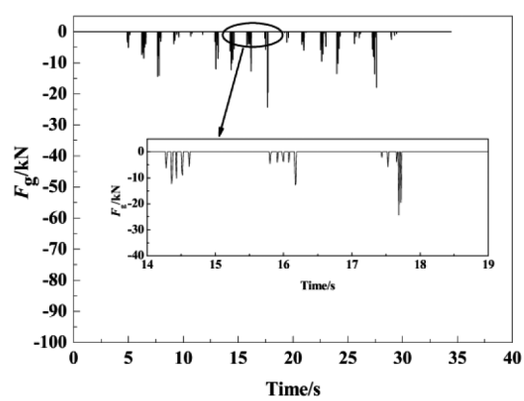

Fig. 6: Transverse force waveforms of the 3rd-axis inner wheels of the 4th car on the guard rail

Flangeway width/mm	65		70		75	
Item	Calculated maximum	Measured maximum	Calculated maximum	Measured maximum	Calculated maximum	Measured maximum
F_g/kN	33.06	32.91	17.61	17.54	9.31	9.20
F_f/kN	52.03	57.01	70.55	72.71	88.51	89.38
$F_g/(F_g+F_f)$/%	38.81	36.6	19.98	19.43	9.52	9.33
y_g/mm	5.09	5.60	4.39	4.80	3.10	3.60
y_{or}/mm	5.13	5.90	6.67	7.20	8.23	8.90

Table 2 Comparison of the theoretical calculation results and the measured results

Figs. 5 and 6 show the transverse force waveforms of the 1st-axis and 3rd-axis inner wheels of the 4th car on the guard rail, respectively. Some degree of impact can be observed in both Figs. 5 and 6, which show the contact randomness between the inner wheel and the guard rail when the train is running. The maximum lateral forces of the 1st axis and 3rd axis inner wheels of the 4th car on the guard rail were 33.06 and 24.30 kN, respectively. The negative values indicate that the force direction in Fig. 3 in the forward direction is opposite to the coordinate system. The maximum transverse force on the guard rail occurred on the 1st axis at 33.06 kN.

Figs. 7 and 8 show the flange force waveforms of the 1st-axis and 3rd-axis outer wheels of the 4th car on the guard rail, respectively. Some degree of impact can be observed. The maximum flange forces of the 1st-axis and 3rd-axis outer wheels are 52.03 and 44.35 kN, which also occur on the 1st-axis of the 4th car. Furthermore, the transverse impact on the guard rail and the flange force point to the same directions, thus enabling the guard rail to share flange force. This phenomenon can decrease the interaction force between the outer wheel flange and the outer rail significantly, thus reducing outer rail abrasion.

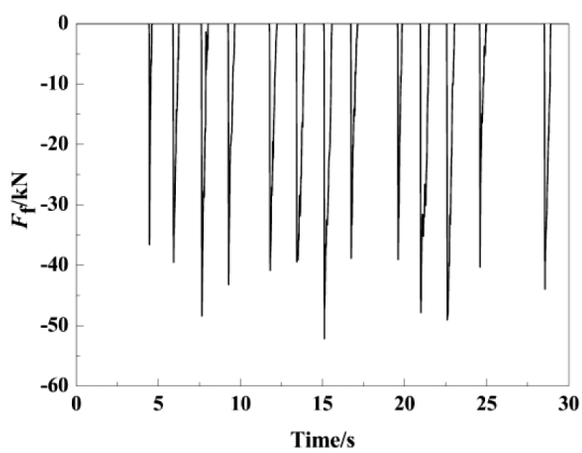

Fig. 7: Flange force waveforms of the 1st-axis outer wheels of the 4th car on the outer rail

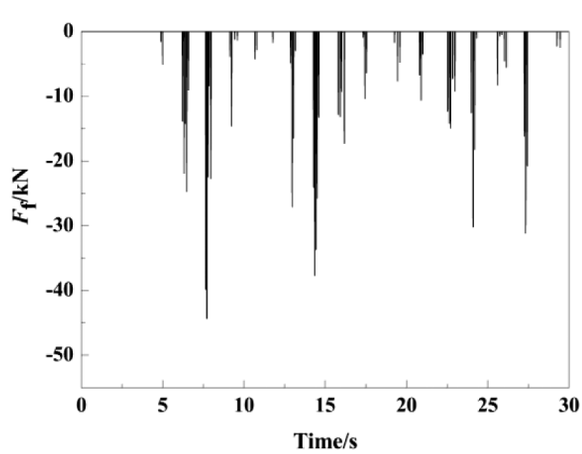

Fig. 8: Flange force waveforms of the 3st-axis outer wheels of the 4th car on the outer rail

The variation curve of lateral displacements of the guard rail (y_g) at the curve rail 200 m away from the calculation start against the distance is presented in Fig. 9. The guard rail at the test point comes in contact with the back of several inner wheels, which makes it had transverse elastic deformation. The maximum lateral displacement of the guard rail is 5.09 mm, which is close to the measured maximum (5.60 mm). Guard rail transverse and lateral deformation can reduce the curve of the outer side rail and prevent abrasion and wear.

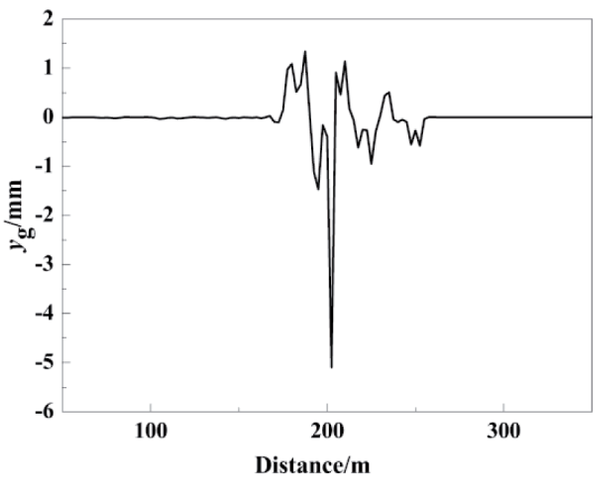

Fig. 9: Variation curve of y_g at the curve rail 200 m away from the calculation start against the distance

Fig. 10 is the time-history curve of lateral Sperling stability index of the 4th car. Generally, the lateral Sperling stability index of the train changes greatly before and after the installation of a new guard rail device and it was greater than that after the installation of a new guard rail device. When there is no new guard rail, the maximum lateral Sperling stability index is 5.01, which is higher than the smooth running standard (4.25, qualified) of freight train (GB5599-85)[18]. When there is a new guard rail, the maximum value is 4.54, which is close to the standard. This reveals that installing the new guard rail at the inner side of the curve rail can indeed improve the riding stability of freight train.

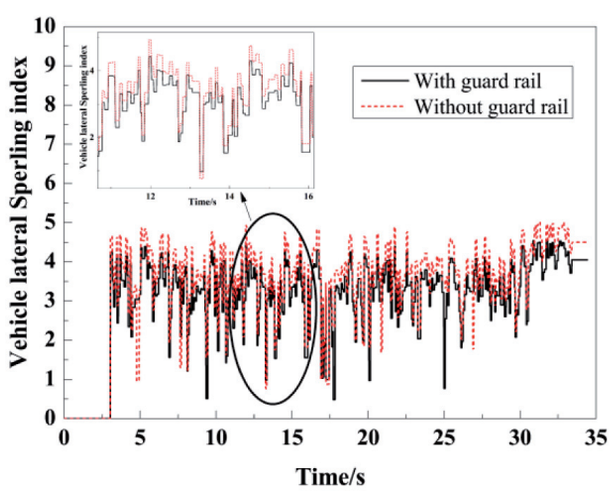

Fig. 10: Time-history curve of the lateral Sperling stability index of the 4th car

Fig.11 shows the variation curves of lateral displacement of the outer rail (y_{or}) at the point 200 m away from the calculation start when there is a new guard rail and when there is no new guard rail on the curve rail. The maximum lateral displacement of the outer rail when the new guard rail is installed on the curve rail is 5.13 mm, but that when there is no new guard rail is 6.01 mm. Thus, under same test conditions and parameters, lateral displacement of the outer rail decreases by 14.64% after the installation of the new guard rail. This indicates that the new guard rail device can effectively reduce the lateral displacement of the outer rail of the curve and increase the lateral stability of the track structure.

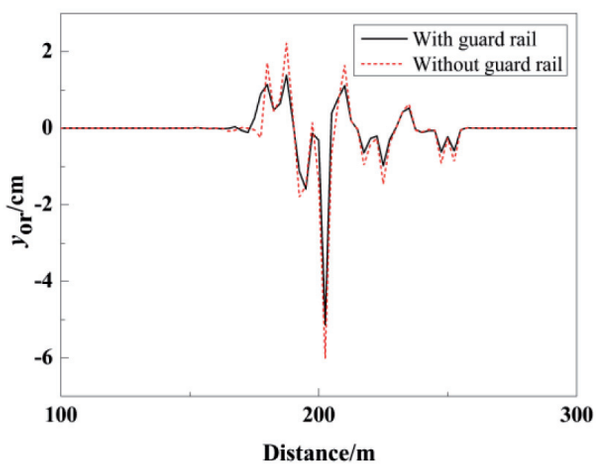

Fig. 11: Variation curves of y_{or} at 200 m away from the calculation start

Given that other parameters are fixed, the guard rail force and flange force at 250, 300, 350 , 400, 450, 500 and 600 m curve radii as well as the corresponding elevation of curves are shown in Fig.12. As can be seen, both guard rail force and flange force decrease with the increase of curve radius. The proportion of flange force shared by the guard rail force is reduced accordingly. The proportions of the transverse impact on the outer rail of the curve shared by the new guard rail are 39.94%, 38.81%, 36.71% , 35.88% , 34.87%, 33.58% and 33.10% at curve radii of 250, 300, 350 , 400, 450, 500 and 600 m, respectively. These results agree with the test conclusion that the new guard rail can share 33.3%–40% flange force of the outer rail of the curve. This further confirms the validity of the established model and calculation.

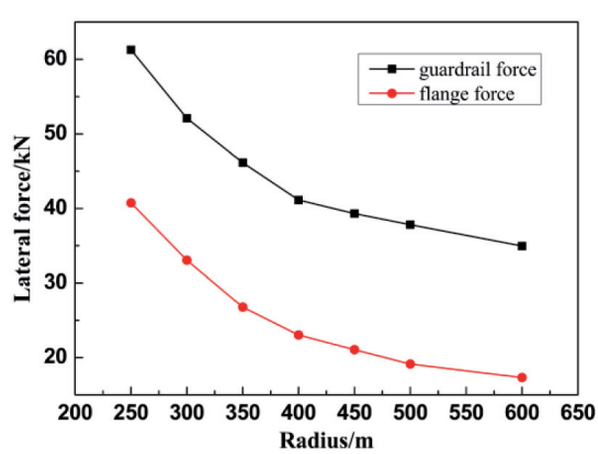

Fig. 12: Variation curves of guard rail force and flange force with radius

5. CONCLUSIONS

Based on the structural characteristics of the new guard rail and geometric contact state, as well as interaction between the guard rail and wheels, a spatial vibration model of train-curve rail system with new guard rail is established. FORTRAN language is used to compile corresponding calculation program. A simulation analysis is conducted to evaluate the space vibration of the train-curve rail system with new guard rail device. Meanwhile, the effect of the new guard rail on the space vibration response of train-rail system is analyzed. The main conclusions of this paper are presented below:

(1) Spatial vibration response the train-curve rail system with new guard rail device is calculated. According to the results of the field dynamic test, the proposed method to calculate the space vibration of the train-curve rail system with the new guard rail device and the corresponding calculation program is valid and feasible.

(2) Installing the new guard rail device at the inner side of curve rails effectively decreased flange force and lateral displacement at the outer rail of the curve, thus reducing steel abrasion and maintenance. The lateral Sperling stability index of the train proves that the new guard rail can significantly improve the riding stability of the freight train.

(3) Guard rail force and flange force decreased with the increase of curve radius. The proportion of flange force shared by the guard rail force also decreased to a certain extent. The proportions of the transverse impact on the outer rail of the curve shared by the new guard rail are 39.94%, 38.81%, 36.71% , 35.88% , 34.87%, 33.58% and 33.10% at curve radii of 250, 300, 350, 400, 450, 500 and 600 m, respectively. These results agree with the test conclusion that the new guard rail can share 33.3%–40% flange force of the outer rail of the curve.

6. APPRECIATION

This research was funded by the National Natural Science Foundation of China and Shenhua Group No.U1261113, Specialized Research Fund for the Doctoral Program of Higher Education of China No.20100162110022, Open Project of Traction Power State Key Laboratory of Southwest Jiaotong University No.TPL1214, the Jiangxi Science Foundation for Youths No.20142BAB216003, and the Natural Science Foundation of China for Youths No.51208198.

BIBLIOGRAPHY

[1] Li Z C. " Analysis of practical effect of the new guard rail ". *Railway Engineering*. February 2014. Vol. 28-1.p.106-108. DOI: 10.3969/j.issn.1003-1995.2014.01.30 (in Chinese)

[2] Ran L, Feng J, Li J X. " Design on derailment guard rail device for elevated bridge in urban mass transit " . *Railway Standard Design*. April 2011. Vol. 55-1.p.42-44. DOI:10.3969/j.issn.1004-2954.2011.01.015(in Chinese)

[3] Chen X S. " Calculation and discussion about width of rim notch of wheel-protecting track ". *Hebei Metallurgy*. May 2009. Vol. 20-5.p.57-59. DOI:10.3969/j.issn.1006-5008.2009.05.023(in Chinese)

[4] Wu F L,Pang G B,Ren J J,et al. " Finite Element analysis and design improvement of small-radius curve anti-friction rail protector ". *Journal of Taiyuan University of Technology*. January 2001. Vol.32-2.p.164-166. DOI: 10.3969/j.issn.1007-9432.2001.02.018(in Chinese)

[5] Arnold M, Burgermeister B, Führer C, et al. " Numerical methods in vehicle system dynamics: state of the art and current developments ". *Vehicle System Dynamics*. July 2011. Vol.49-7.p.1159-1207. DOI:10.1080/00423114.2011.582953

[6] Jin X S, Xiao X B, Ling L, et al. " Study on safety boundary for high-speed train running in severe environments ". *International Journal of Rail Transportation*. February 2013. Vol.1-2.p.87-108. DOI:10.1080/23248378.2013.790138

[7] Eom B G, Lee H S. " Assessment of running safety of railway vehicles using multibody dynamics". *International Journal of Precision Engineering and Manufacturing*. April 2010. Vol.2-11.p.315-320. DOI: 10.1007/s12541-010-0036-x

[8] Wilson N, Fires R, Witte M, et al. " Assessment of safety against derailment using simulations and vehicle acceptance tests: a worldwide comparison of state-of-the-art assessment methods". *Vehicle System Dynamics*. July 2011. Vol.49-7. p.1113-1157. DOI:10.1080/ 00423114.2011.586706

[9] Hung C, Suda Y, Aki M, et al. " Study on detection of the early signs of derailment for railway vehicles". *Vehicle System Dynamics*. December 2010, Vol.48-12.p.451-466. DOI:10.1080/00423114.2010.486862

[10] Mohammadzadeh S, Sangtarashha M, Molatefi H. " A novel method to estimate derailment probability due to track geometric irregularities using reliability techniques and advanced simulation methods". *Archive of Applied Mechanics*. November 2011. Vol.81-11.p.621-1637. DOI: 10.1007/s00419-011-0506-3

[11] Xiang J, Li D J, Zeng Q Y. " Simulation of spatially coupling dynamic response of train track time variant system ". *Journal of Central South University of Technology*. September 2003. Vol.10-3.p.226-230. DOI:10.1007/s11771-003-0014-x

[12] Xiang J, Zeng Q Y, Lou P. " Transverse vibration of train-bridge and train-track time-variant system and the theory of random energy analysis for train derailment ". *Vehicle System Dynamics*. January 2004, Vol.41-2.p.129-155. DOI:10.1076/vesd.41.2.129.26499

[13] LI Z C, Zhang A J, Song N. " Installation and use of new type elastic wear-reducing derail-preventing guard rail device ". *Railway Engineering*. October 2013. Vol.20-10.p.120-122. DOI: 10.3969/j.issn.1003-1995.2013.10.37 (in Chinese)

[14] Ren Z S, Zhai W M, Wang Q C. " Simulation calculation of lateral impact force acting on guard rail while passing through turnout zone on the side-way ". *Journal of Southwest Jiaotong University*. February 2000. Vol.35-4.p.344-347. DOI:10.3969/j.issn.0258-2724.2000.04.003 (in Chinese)

[15] Remco I, Leine, Nijmeijer, et al. *Dynamics and bifurcations of non-smooth mechanical systems* . Germany: Springer, 2004. 236 p.ISBN: 3540219870

[16] Zeng Q Y, Lou P, Xiang J. " The principle of total potential energy with stationary value in elastic system dynamics and its application to the analysis of vibration and dynamic stability ". *Journal of Huangzhong University of Science & Technology (Urban Science Edition)*. January 2002. Vol.35-1.p.7-14. DOI:10.3969/j.issn.2095-0985.2002.01.003

[17] Bureau of Beijing Railway, China Academy of Railway Sciences. *Dynamical test report of the new guard rail in small radius curve tracks* . Beijing: China Academy of Railway Sciences,2000. 20 p. (in Chinese)

[18] General Administration of Quality Supervision, Inspection and Quarantine of the People's Republic of China, Standardization Administration of the People's Republic of China. *Railway Vehicles-S Pecification for Evaluation the Dynamic Performance and Accreditation Test* . Beijing: China Railway Publishing House, 1986. 32 p. ISBN:15506613872 (in Chinese)